

HELICITY OBSERVATIONS OF WEAK AND STRONG FIELDS

MEI ZHANG¹

Received 2006 April 2; accepted 2006 June 8; published 2006 July 14

ABSTRACT

We report in this Letter our analysis of a large sample of photospheric vector magnetic field measurements. Our sample consists of 17,200 vector magnetograms obtained from 1997 January to 2004 August by the Huairou Solar Observing Station of the Chinese National Astronomical Observatory. Two physical quantities, α and current helicity, are calculated, and their signs and amplitudes are studied in a search for solar cycle variations. Differently from other studies of the same type, we calculate these quantities for weak ($100 \text{ G} < |B_z| < 500 \text{ G}$) and strong ($|B_z| > 1000 \text{ G}$) fields separately. For weak fields, we find that the signs of both α and current helicity are consistent with the established hemispheric rule during most years of the solar cycle and that their magnitudes show a rough tendency of decreasing with the development of the solar cycle. The analysis of strong fields gives an interesting result: both α and current helicity present a sign opposite to that of weak fields. The implications of these observations for dynamo theory and helicity production are also briefly discussed.

Subject headings: MHD — Sun: interior — Sun: magnetic fields

1. INTRODUCTION

Magnetic helicity is a physical quantity that measures the topological complexity of a magnetic field, such as the degree of linkage and/or twistedness in the field (Moffatt 1985; Berger & Field 1984). It has been shown that its total amount is approximately conserved in the Sun even when there is an energy release during fast magnetic reconnection (Berger 1984). This conservation of total magnetic helicity is considered to play an important role in the dynamical processes in the Sun. For example, by considering helicity conservation in the mean-field dynamo, theories have predicted that the solar dynamo would produce opposite helicity signs in the mean field and in the fluctuations (Blackman & Field 2000; see Ossendrijver 2003 for a review). It has also been considered that magnetic helicity and its conservation may play an important role in CME dynamics (Low 2001; Demoulin et al. 2002), where accumulation of total magnetic helicity in the respective northern and southern hemispheres leads to a natural magnetic energy storage for CME eruptions (Zhang & Low 2005; Zhang et al. 2006).

A direct measurement of magnetic helicity and hence a direct test of the above theories by observations are still out of our reach because so far the photosphere is the only layer in which we can measure vector magnetic fields with reasonable temporal and spatial resolutions. However, by calculating derived physical quantities, such as α and current helicity, from the observed photospheric vector magnetograms we do get a glimpse of properties of magnetic helicity in the Sun. For example, from photospheric magnetic field measurements we learn that magnetic fields emerging from the solar convection zone into the photosphere are already significantly twisted (Kurokawa 1987; Leka et al. 1996), and statistically these fields possess a positive helicity sign in the southern hemisphere and a negative helicity sign in the northern hemisphere (Pevtsov et al. 1995; Bao & Zhang 1998). These observations thus provide us implications on how magnetic helicity might be produced in the convection zone (Berger & Ruzmaikin 2000) and how magnetic helicity conservation might have played a role in balancing the twist and writhe helicity in an originally untwisted flux rope (Longcope et al. 1998).

In this Letter, we intend to use photospheric vector magnetic field measurements to find further observational indications of helicity production and conservation. Differently from other works of the same type, we separate the studied fields into two parts: strong magnetic fields and weak magnetic fields. We organize our paper as follows: In § 2 we describe our observations and data reduction. In § 3 we present our analysis and discussion. We conclude the Letter with a brief summary in § 4.

2. OBSERVATIONS AND DATA REDUCTION

The tunable birefringent filter of the solar telescope magnetograph at the Huairou Solar Observing Station of the Chinese National Astronomical Observatory can be aimed at different passbands for different observations (Ai & Hu 1986). For photospheric observations the passband of the filter is set in the Fe I $\lambda 5324$ line: at 0.075 \AA from the line center for the measurement of the longitudinal magnetic field (Stokes V) and at the line center for the measurement of transverse magnetic fields (Stokes Q and U). More information of the magnetograph and calibration can be found in Ai et al. (1982) and Zhang & Ai (1986).

A data set of photospheric vector magnetograms obtained with the above magnetograph during the period of 1997 January 1 to 2004 August 31 is analyzed in this Letter. This data set contains 17,200 vector magnetograms and covers almost all active regions that appeared during this period. We calibrate each vector magnetogram according to Ai et al. (1982) and solve the 180° ambiguity by setting the directions of the transverse fields most closely to a current-free field.

We calculate two physical quantities, α and current helicity, of each magnetogram, as helicity proxies. We calculate α either as a best-fit single value α_{best} following Pevtsov et al. (1995) or as a mean value $\langle \alpha_z \rangle$ of the local $\alpha_z = (\nabla \times \mathbf{B})_z / B_z$ as in Pevtsov et al. (1994). The two α -values so calculated are both indicators of the twistedness of the measured field, and there is a linear relationship between them when derived from the same set of magnetograms (Burnette et al. 2004). We use α_{best} in § 3.1 in comparison with Pevtsov et al. (2001) and $\langle \alpha_z \rangle$ in §§ 3.2 and 3.3 because $\langle \alpha_z \rangle$ is presumably less dependent on the linear force-free assumption. The current helicity is calculated as $h_c = B_z \cdot (\nabla \times \mathbf{B})_z$, which is actually the longitudinal

¹ National Astronomical Observatory, Chinese Academy of Sciences, A20 Datun Road, Chaoyang District, Beijing 100012, China; zhangmei@bao.ac.cn.

(z) component of the current helicity density at the photosphere ($z = 0$). When calculating these quantities we have used only those magnetograms whose longitudes are less than 40° from the disk center and only those data points whose longitudinal flux densities ($|B_z|$), after the correction of projection effect, are greater than 100 G and whose transverse flux densities ($|B_x|$ and $|B_y|$) are both greater than 200 G. Note that our treatment of data reduction so far is typical of that of most other authors in reducing vector magnetograms (Pevtsov et al. 1994, 1995, 2001; Bao & Zhang 1998).

Our unique treatment of the data is that we divide our studied fields into two parts: strong magnetic fields whose longitudinal flux densities ($|B_z|$) are greater than 1000 G, and weak magnetic fields whose longitudinal flux densities ($|B_z|$) are between 100 and 500 G. By this definition, our strong fields mainly consist of the umbra of sunspots, and our weak fields of the enhanced magnetic networks around sunspots. We calculate α and current helicity for such defined strong and weak fields separately. Note that by doing so, not only do we gain the opportunity to study the possible differences between weak and strong fields within active regions, but also we get a chance to learn indicated helicity properties of the global Sun if we identify our observed weak fields as representatives of the general weak fields distributed over the entire surface.

3. ANALYSIS AND DISCUSSION

3.1. Comparison with Previous Studies

Before we proceed to presenting our results, it is useful to check our data reduction of this data set with previous results obtained by other instruments and data sets. We select a subsample of our data set containing observations made between 1997 July and 2000 September in order to compare with Pevtsov et al. (2001), who also calculated α_{best} and current helicity for the same period of time. The difference is that their magnetograms were obtained by the Haleakala Stokes Polarimeter (HSP) at Mees Solar Observatory.

Figure 1 presents the latitudinal profile of α_{best} for the 391 active regions observed with the Huairou magnetograph during this period of time. Each point presents the average value of α_{best} when multiple magnetograms of the same active region were obtained. Note that in producing this figure we did not separate the weak and strong fields but instead used all data points with $|B_z| > 100$ G and $|B_x|, |B_y| > 200$ G in order to make a reasonable comparison with Pevtsov et al. (2001). The green line shows the least-squares best-fit linear function of these α_{best} values. The similarity between our figure and Figure 1 of Pevtsov et al. (2001) indicates consistency between the two data sets.

Out of our 391 active regions during this period, 58.9% of 214 active regions in the northern hemisphere have $\alpha_{\text{best}} < 0$ and 67.2% of 117 active regions in the southern hemisphere have $\alpha_{\text{best}} > 0$. These numbers are consistent with the numbers of 62.9% and 69.9% for the northern and southern hemispheres, respectively, in Pevtsov et al. (2001). Our data shows no tendency of hemispheric rule by current helicity; 44.4% of 214 active regions in the northern hemisphere have $h_c < 0$ and 45.8% of 117 active regions in the southern hemisphere have $h_c > 0$. Note that in Pevtsov et al. (2001) a much weaker tendency is also found with numbers of 50% and 57.5% for their h_c values in the northern and southern hemispheres, respectively. They contribute this difference to Faraday rotation. But we suggest that the difference is largely (although possibly not all) because of a physical point, which we will address below.

Averages of α_{best} for active regions observed in each 10° of

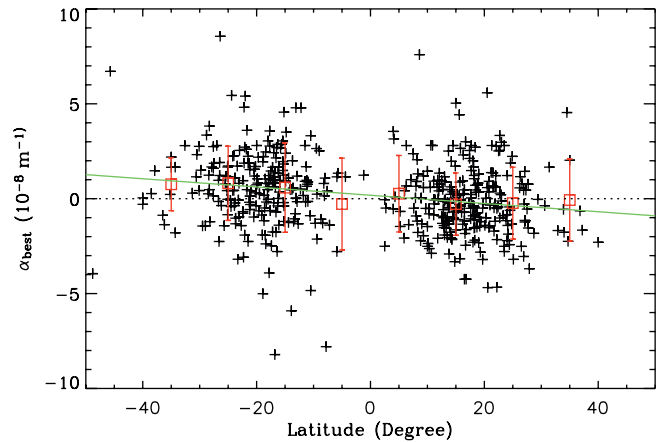


FIG. 1.—Latitudinal profile of α_{best} for the 391 active regions observed by the Huairou magnetograph between 1997 July and 2000 September.

solar latitude are also plotted in Figure 1, presented as red squares. The large error bars of these averages remind us that our established hemispherical rule is of a statistical result. Individual active regions may present large deviations from the mean values. This is also true for other statistical results that we present below.

3.2. Helicity Observations of Weak Fields

Figure 2 presents our result of solar cycle variations of α (top) and current helicity (middle) for weak fields ($100 \text{ G} < |B_z| < 500 \text{ G}$). Each point in these plots is a weighted average of $\langle \alpha_z \rangle$ or current helicity for active regions observed during 1 year. For active regions in the southern hemisphere the weight is set to 1 and for active regions in the northern hemisphere the weight is set to -1 . The weighted averages then indicate the magnitudes of α or current helicity averaged over the global surface during an entire year, assuming the northern and southern hemispheres have opposite helicity signs. We see that both averaged α and current helicity have positive signs except for the year 2004. This tells us that both α and current helicity for weak fields obey the established hemispheric rule during most years of the solar cycle. The averaged α and current helicity for the year 2004 are negative, which indicates that the usual hemispheric rule is not followed in this year. This is consistent with Hagino & Sakurai (2005), who also found a violation of the usual hemispheric rule during solar minimums.

Figure 2 also presents a rough tendency of a decrease of α and current helicity with the development of solar cycle. We note that in Berger & Ruzmaikin (2000) the helicity production rate by differential rotation in the solar interior is calculated and that their calculations show a similar decrease in magnitude of the rate of helicity transported into the northern and southern hemispheres. This can be seen from the bottom panel of Figure 2, where the helicity transportation rate into the southern hemisphere by the $m = 0$ mode is replotted with data taken from Berger & Ruzmaikin (2000). This interesting consistency seems to suggest that differential rotation is the source of helicity production in the solar interior, although we are not able to make a conclusion because we do not know whether the α -effect will also produce the same tendency or not.

As pointed out by the careful referee, the calculated transferred helicity ends at zero during solar minimums, whereas our observations as well as those of Hagino & Sakurai (2005) show that the helicity goes to the opposite sign during solar

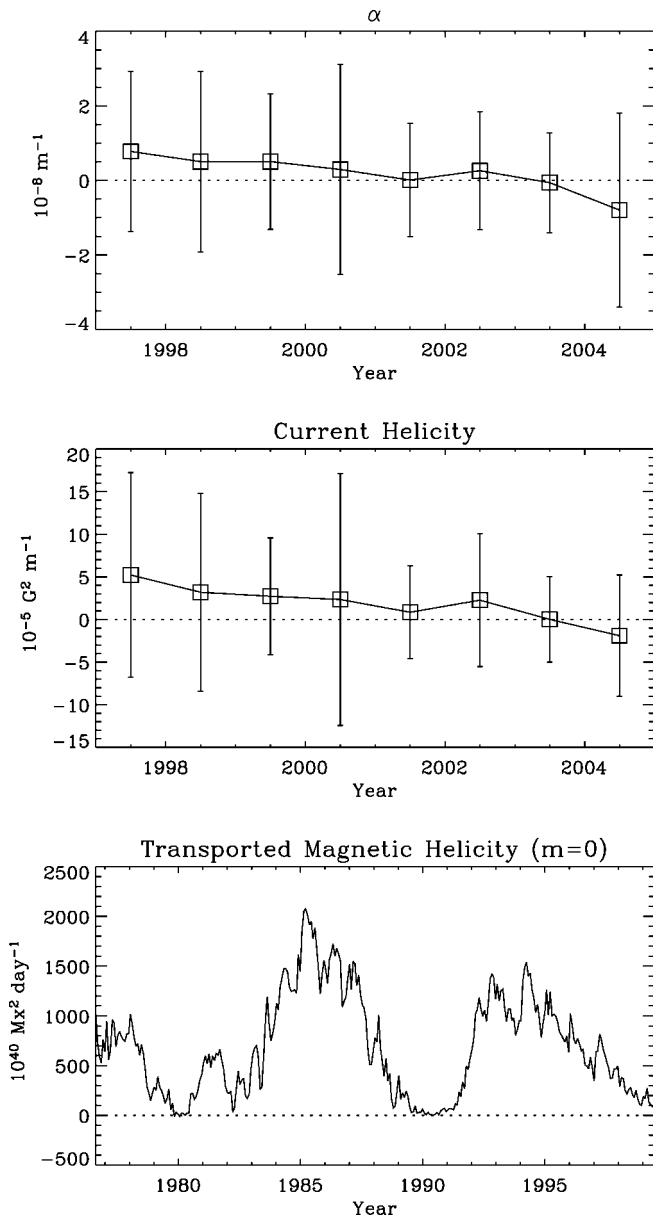


FIG. 2.—Solar cycle variations of weighted averages of α (top) and current helicity (middle) for weak fields ($100 \text{ G} < |B_z| < 500 \text{ G}$). Bottom: Calculated transfer rate of $m = 0$ mode helicity, created by differential rotation in the interior, into the southern hemisphere. Adopted from Berger & Ruzmaikin (2000).

minima. We intend to explain this as a result of transequatorial reconnection (Pevtsov 2000) that has consumed the helicity of the dominate sign in each hemisphere, a point interesting in itself but which is out of the scope of the current Letter.

Another interesting implication of Figure 2 is that whereas we usually consider helicity variation as a function of latitude, as presented in Figure 1, another possibility is that helicity variation is more associated with solar cycle dependence and that the latitude dependence is just a derived relation from this solar cycle dependence of helicity and the butterfly diagram.

3.3. Helicity Observations of Strong Fields

For strong magnetic fields ($|B_z| > 1000 \text{ G}$), the calculation of weighted averages of α and current helicity presents an interesting result, as shown in Figure 3. Both averaged α and current helicity are negative, which means they do not follow

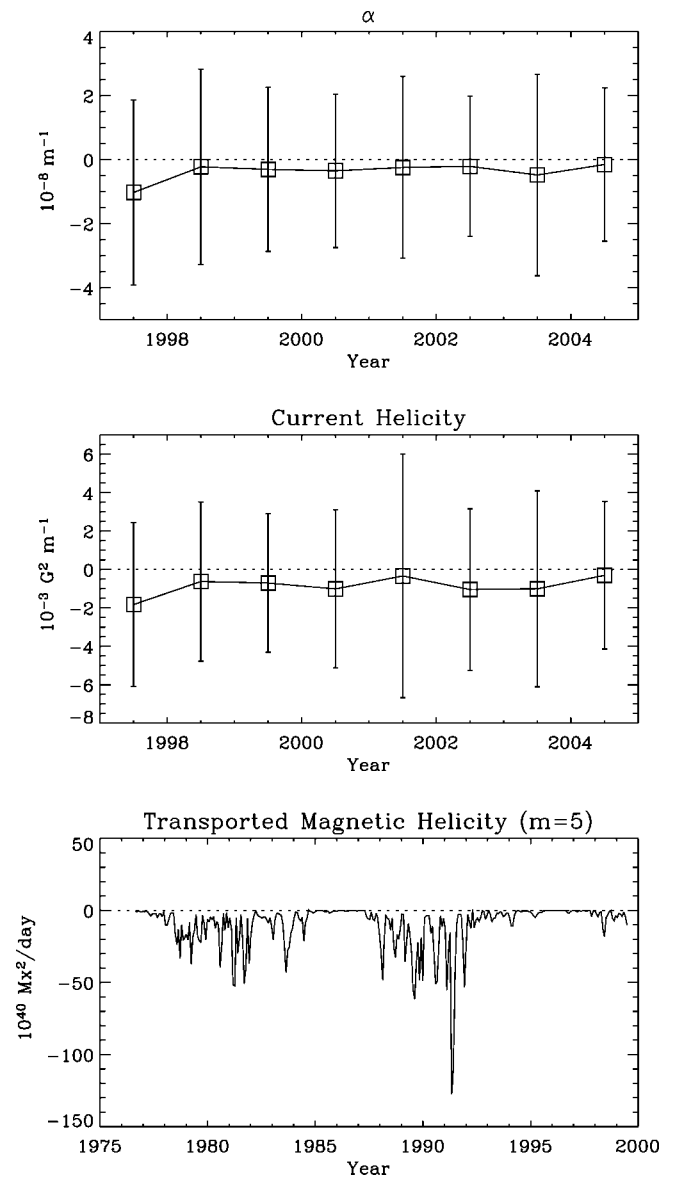


FIG. 3.—Top and middle: Same as in Fig. 2 but for strong fields ($|B_z| > 1000 \text{ G}$). Bottom: Same as in Fig. 2 but for $m = 5$ mode.

the usual hemispheric rule. This also means that strong fields have a helicity sign opposite to that of weak fields.

As we mentioned earlier, if we interpret our observed weak fields in active regions as representatives of the general weak fields distributed over the global Sun, then we can use them to represent the large-scale field. Our strong fields may be used to represent the small-scale fluctuations compared to the large-scale of the global Sun. Then under this interpretation our observations seem to be consistent with the theory that the solar dynamo would produce opposite helicity signs in the mean field and in the fluctuations.

It is also interesting to note that in Berger & Ruzmaikin (2000) the higher mode helicities, such as the $m = 5$ mode replotted in Figure 3, also has a sign opposite to that of the $m = 0$ mode. Again, if we interpret their low-degree (such as $m = 0$) mode field as corresponding to our weak field because both of them represent a more uniformly distributed field over the global Sun, and if we interpret their high-degree (such as $m = 5$) mode field as corresponding to our strong field because both of them appear sporadically on the surface, then their calculations and our observations show consistency again.

The observation that strong fields have a helicity sign opposite to that of weak fields may help us understand why α_{best} usually shows a better hemispheric rule than current helicity if both quantities are calculated from vector magnetograms of the whole field (Pevtsov et al. 2001). We interpret this as follows. When we calculate α_{best} of the entire field, each data point is given an equal weight. This results in the calculated α_{best} presenting the sign of weak fields, whose number of data points dominates over that of strong fields. But when we calculate the current helicity of the entire field, defined as $h_c = B_z \cdot (\nabla \times \mathbf{B})_z = \alpha B_z^2$, we have attributed a weight of B_z^2 to each data point. This then results in a near cancellation of current helicity between the weak and strong fields because weak and strong fields happen to have opposite helicity signs and the former has a larger number of data points but smaller B_z^2 values for each data point whereas the latter has a smaller number of data points but each data point has a larger B_z^2 value.

It has been suggested that Faraday rotation contributes to the difference between α_{best} and current helicity. We suggest that the main reason is the opposite helicity signs between weak and strong fields. J. T. Su & H. Q. Zhang (2006, in preparation) recently did a calculation and showed that whereas Faraday rotation may rotate the transverse fields by 20° – 30° , the resultant α -values are less influenced, with changes of α -values all less than a few percent. Another comment is that if Faraday rotation is the reason for the difference, we should not see the difference in the data set obtained by spectrograph-type magnetographs, where the effect of Faraday rotation can be taken care of by inversion methods. But the difference is observed in Pevtsov et al. (2001), who used HSP data. We have recently checked several active regions observed with the Advanced Stokes Polarimeter (ASP) at the High Altitude Observatory. A similar feature of opposite helicity signs between weak and strong fields is found, although not in every region examined. As also kindly pointed out by the referee, a similar tendency of opposite helicity signs is indicated in a decaying active region observed with the ASP (Fig. 4 of Pevtsov & Canfield 1999).

Finally, we point out another consistency between our observations and previous studies. By applying a known reconstruction technique to Michelson Doppler Imager data, Pevtsov & Latushko (2000) calculated the current helicity of the global

Sun. They found that the usual hemispheric rule is followed for regions above 40° of solar latitude whereas the rule is surprisingly not obvious for regions within 40° of solar latitude. With our observations, we now can interpret this as follows. In high latitudes magnetic fields are dominated by weak fields with their signs following the usual hemispherical rule, whereas in low latitudes strong fields with an opposite helicity sign are present, resulting in a reduction of the usual hemispherical rule.

4. SUMMARY

A large sample of 17,200 photospheric vector magnetograms of active regions obtained from 1997 January to 2004 August is analyzed in this Letter. Differently from other works, we calculate the helicity proxies, α and current helicity, for weak ($100 \text{ G} < |B_z| < 500 \text{ G}$) and strong ($|B_z| > 1000 \text{ G}$) fields separately.

By analyzing this data set we find the following: (1) For weak magnetic fields, the signs of both α and current helicity follow the established hemispheric rule except during the year 2004. The magnitudes of their weighted averages show a weak tendency of decreasing with the development of the solar cycle. (2) For strong magnetic fields, both α and current helicity show a helicity sign opposite to that of weak fields.

Our results seem to be consistent with the theoretical prediction that the solar dynamo would produce opposite helicity signs in the mean field and in the fluctuations, as well as with the theoretical calculations of helicity production rate by differential rotation. However, as pointed out by the referee, some previous studies (Longcope et al. 1998, 1999; Chae 2001) have suggested that neither the interface dynamo nor the differential rotation would generate sufficient amount of helicity (twist). So our observation with its interesting implications advocates further investigations, both observationally and theoretically.

I thank Mitchell Berger for providing his calculation data used in this Letter. I also thank the anonymous referee for helpful comments and suggestions. This work was supported by the One Hundred Talent Program of the Chinese Academy of Sciences, the Chinese National Science Foundation under grant 10373016, and the US National Science Foundation under grant ATM 05-48060.

REFERENCES

- Ai, G., & Hu, Y. 1986, *Acta Astron. Sinica*, 27, 173
 Ai, G., Li, W., & Zhang, H. 1982, *Chinese Astron. Astrophys.*, 6, 129
 Bao, S., & Zhang, H. Q. 1998, *ApJ*, 496, L43
 Berger, M. A. 1984, *Geophys. Astrophys. Fluid Dyn.*, 30, 79
 Berger, M. A., & Field, G. B. 1984, *J. Fluid Mech.*, 147, 133
 Berger, M. A., & Ruzmaikin, A. 2000, *J. Geophys. Res.*, 105, 10481
 Blackman, E. G., & Field, G. B. 2000, *MNRAS*, 318, 724
 Burnette, A. B., Canfield, R. C., & Pevtsov, A. A. 2004, *ApJ*, 606, 565
 Chae, J. 2001, *ApJ*, 560, L95
 Demoulin, P., et al. 2002, *A&A*, 382, 650
 Hagino, M., & Sakurai, T. 2005, *PASJ*, 57, 481
 Kurokawa, H. 1987, *Sol. Phys.*, 113, 259
 Leka, K. D., Canfield, R. C., McClymont, A. N., & van Driel-Gesztelyi, L. 1996, *ApJ*, 462, 547
 Longcope, D. W., Fisher, G. H., & Pevtsov, A. A. 1998, *ApJ*, 507, 417
 Longcope, D. W., et al. 1999, in *Magnetic Helicity in Space and Laboratory Plasmas*, ed. M. R. Brown et al. (Geophys. Monogr. 111; Washington: AGU), 93
 Low, B. C. 2001, *J. Geophys. Res.*, 106, 25141
 Moffatt, H. K. 1985, *J. Fluid Mech.*, 159, 359
 Ossendrijver, M. 2003, *A&A Rev.*, 11, 287
 Pevtsov, A. A. 2000, *ApJ*, 531, 553
 Pevtsov, A. A., & Canfield, R. C. 1999, in *Magnetic Helicity in Space and Laboratory Plasmas*, ed. M. R. Brown et al. (Geophys. Monogr. 111; Washington: AGU), 103
 Pevtsov, A. A., Canfield, R. C., & Latushko, S. M. 2001, *ApJ*, 549, L261
 Pevtsov, A. A., Canfield, R. C., & Metcalf, T. R. 1994, *ApJ*, 425, L117
 ———. 1995, *ApJ*, 440, L109
 Pevtsov, A. A., & Latushko, S. M. 2000, *ApJ*, 528, 999
 Zhang, H. Q., & Ai, G. X. 1986, *Acta Astron. Sinica*, 27, 217
 Zhang, M., Flyer, N., & Low, B. C. 2006, *ApJ*, 644, 575
 Zhang, M., & Low, B. C. 2005, *ARA&A*, 43, 103